Food Chemistry 420 (2023) 136083

Contents lists available at ScienceDirect

Food Chemistry

journal homepage: www.elsevier.com/locate/foodchem

Enhanced anode electrochemiluminescence in split aptamer sensor for kanamycin trace monitoring

Xiaoyue Zhang [a], Yu Du [a], Xuejing Liu [a], Rui Feng [d], Yue Jia [a], Xiang Ren [a], Nuo Zhang [a], Lei Liu [a,*], Qin Wei [a,b,*], Huangxian Ju [a,c]

[a] Key Laboratory of Interfacial Reaction & Sensing Analysis in Universities of Shandong, Collaborative Innovation Center for Green Chemical Manufacturing and Accurate Detection, School of Chemistry and Chemical Engineering, University of Jinan, Jinan 250022, China
[b] Department of Chemistry, Sungkyunkwan University, Suwon 16419, Republic of Korea
[c] State Key Laboratory of Analytical Chemistry for Life Science, Department of Chemistry, Nanjing University, Nanjing 210023, China
[d] School of Water Conservancy and Environment, University of Jinan, Jinan 250022, China

ARTICLE INFO

Keywords:
Split aptamer
Electrochemiluminescence
Kanamycin

ABSTRACT

Covalently modifying electrochemiluminescence (ECL) luminophores to alter their energy levels or generate energy/electron transfer processes for improved performance is hindered by the complex design and fabrication processes. In this study, non-covalent bond self-assembly was employed to enhance the ECL property of gold nanoclusters with tryptophan (Try) and mercaptopropionic acid (MPA) as ligands (Try-MPA-gold nanoclusters). Specifically, through the molecular recognition of Try by cucurbit[7]uril, some non-radiative transition channels of the charge carriers on the surface of the Try-MPA-gold nanoclusters were restricted, resulting in a significant enhancement of the ECL intensity of the nanoclusters. Furthermore, rigid macrocyclic molecules acted on the surface of the nanoclusters through self-assembly, forming a passive barrier that improved the physical stability of the nanoclusters in the water-phase and indirectly improved their luminescent stability. As an application, cucurbit[7]uril-treated Try-MPA-gold nanoclusters (cucurbit[7]uril@Try-MPA-gold nanoclusters) were used as signal probes, and Zn-doped SnO_2 nanoflowers (Zn-SnO_2 NFs) with high electron mobility were used as electrode modification material to establish an ECL sensor for kanamycin (KANA) detection, utilizing split aptamers as capture probes. The advanced split aptamer sensor demonstrated excellent sensitivity analysis for KANA in complex food substrates with a recovery rate of 96.2 to 106.0%.

1. Introduction

Kanamycin (KANA) is a broad-spectrum aminoglycoside antibiotic widely used in animal husbandry due to its low cost and good antimicrobial properties. However, the irrational use of KANA in livestock and poultry breeding can lead to residual KANA in animal food, which can enter the human body through the biological circulatory system (Hu, Song, Zhou, Liu, & Lv, 2021; Huang, Li, Chen, Xu, Xie, Deng, et al., 2021). Traditional detection methods for KANA residue include high-performance liquid phase spectrometry (HPLC) and liquid chromatography-tandem mass spectrometry (LC-MS/MS), which are highly sensitive but expensive and complicated. (Robati, Arab, Ramezani, Langroodi, Abnous, & Taghdisi, 2016). Electrochemiluminescence (ECL) sensor is an ideal tool for KANA detection due to its advantages of low background signal, high sensitivity, fast response, low instrument cost, and good controllability (Cheng, Zhang, Huang, Xu, Sun, & Guo, 2020; Jiang, Qin, Zhang, Shan, & Chen, 2021; H. Wang, Wang, Cai, Liu, Zhang, Fang, et al., 2022; Zhang, Wang, Xiong, Huang, Jin, Wang, et al., 2021). As a reliable ECL sensor capture probe, aptamer has been rapidly developed in the field of small molecule sensing due to its advantages of low production cost, fast synthesis speed, and strong affinity (Li, Luo, Cheng, Sun, Zhang, Liu, et al., 2022; Tian, Wang, Zhuang, Wu, Yu, & Ding, 2023; Y. Wang, Feng, & Kan, 2022). However, the long-chain aptamer is prone to fold into a non-specific structure, which makes it difficult to identify the target (Zhao, Qi, Yan, Huang, Liang, Zhang, et al., 2019). Splitting a long-chain complete aptamer into two or more

* Corresponding authors at: Key Laboratory of Interfacial Reaction & Sensing Analysis in Universities of Shandong, Collaborative Innovation Center for Green Chemical Manufacturing and Accurate Detection, School of Chemistry and Chemical Engineering, University of Jinan, Jinan 250022, China; Department of Chemistry, Sungkyunkwan University, Suwon 16419, Republic of Korea (Q. Wei).
E-mail addresses: liulei70919@126.com (L. Liu), sdjndxwq@163.com (Q. Wei).

https://doi.org/10.1016/j.foodchem.2023.136083
Received 15 February 2023; Received in revised form 26 March 2023; Accepted 28 March 2023
Available online 30 March 2023

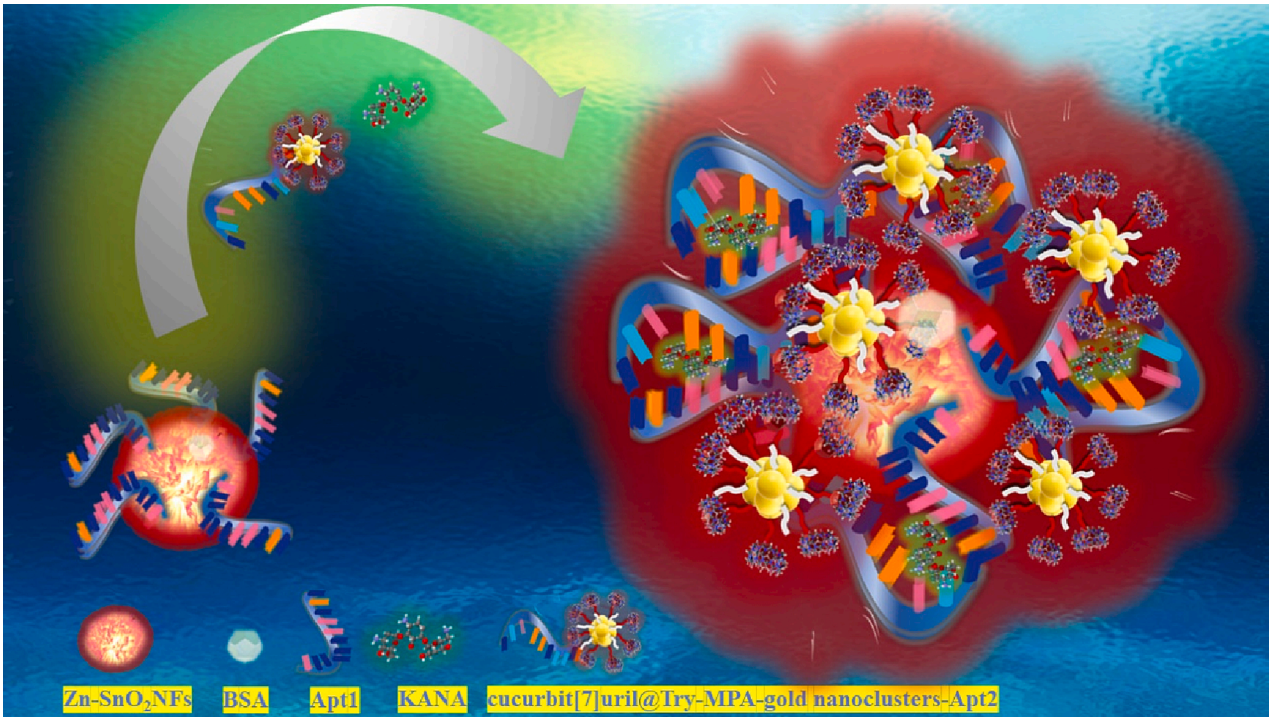

Scheme 1. Schematic diagram of the split aptamer sensors.

aptamer fragments can stabilize the aptamer structure and reduce its flexibility, which can help in identifying the target (Debiais, Lelievre, Smietana, & Müller, 2020; Ye, Yang, Khan, Niazi, Guo, Wang, et al., 2022). Split aptamers can jointly identify the target, which can address the false positive problem caused by the flexible structure of aptamer (Qi, Dong, Sun, Zhang, Duan, & Wang, 2022; R. Wang, Zhang, Zhang, Shi, Nguyen, & Zhou, 2019). Moreover, split aptamers can enrich the design types of aptamer sensors, making it possible to design sandwich aptamer sensors with high sensitivity. To date, no KANA ECL sensor based on split aptamer has been reported. Consequently, the application of split aptamers for KANA identification in ECL sensors is a meaningful research effort (Scheme 1).

Gold nanoclusters are extremely small metallic nanomaterials composed of hundreds of gold atoms and ligands (Guan, Li, Hu, & Wang, 2022; Zheng, Wu, Jiang, & Wang, 2021). They are promising ECL luminophores with the advantages of high biocompatibility (Matus & Häkkinen, 2021), tunable luminescence (He, Huang, & Chen, 2020), and easy labeling (Yu, Zhang, Kang, Zhang, Shen, & Zou, 2020). However, compared to the classic ECL emitters, the ECL performance of gold nanoclusters still needs to be improved. The surface effect has a great influence on the ECL performance of gold nanoclusters. Many dangling bonds will form many non-radiative transition channels on the surface of the gold nanoclusters and trap charge carriers, which will affect the interaction of active intermediates and the radiation relaxation of excited states. Cucurbit[7]uril is a supramolecular host compound with a rigid cavity. Through the molecular recognition of tryptophan (Try) by cucurbit[7]uril (El-Barghouthi, Bodoor, Abuhasan, Assaf, Al Hourani, & Rawashdeh, 2022), cucurbit[7]uril can assemble on the surface of gold nanoclusters with Try and mercaptopropionic acid (MPA) as ligands (cucurbit[7]uril@Try-MPA-gold nanoclusters) to form a supramolecular structure. The macrocyclic molecular cavity structure of cucurbit[7]uril restricts the non-radiative relaxation of the ligands and forms a passivated "supramolecular shell" on the surface. This shell effectively prevents the adsorption of charge carriers on the surface, thereby avoiding potential influence on the nanoclusters. When the cucurbit[7]uril@Try-MPA-gold nanoclusters are used as the signal probe, the sensitivity and stability of the constructed sensor may be significantly improved.

The concentration of electroactive substances at the electrode surface and the electron transmission rate affects the luminescence properties of the ECL system. SnO_2 is a prototype of a "transparent conductor" that displays properties of high metallic conductivity, which is attributed to its massive structural nonstoichiometry. Doping with transition metals can lead to changes in the microstructure of SnO_2, which can enhance some properties of SnO_2. Zn-doped SnO_2 nanoflowers (Zn-SnO_2 NFs) have high electron mobility and excellent chemical stability (Dou, Sabba, Mathews, Wong, Lam, & Mhaisalkar, 2011), which could promote electron transfer between electroactive substances. Moreover, due to surface effects of Zn-SnO_2 NFs, when used as an electrode modification material, more electroactive substances can be adsorbed on the electrode surface.

Based on the above superiorities, an ECL split aptamer sensor with cucurbit[7]uril@Try-MPA-gold nanoclusters as the anode signal probe and Zn-SnO_2 NFs as the electrode modification material for KANA sensitive detection was proposed. The split aptamer sensor achieved excellent sensitivity analysis for KANA.

2. Experimental section

2.1. Materials

The 3-aminopropyl triethoxysilane (APTES) and bovine serum albumin (BSA) (96 ~ 99%) were supplied by Sigma-Aldrich Co. (USA). Prostate specific antigen (PSA) and immune globulin (IgG) were purchased from Shanghai Linc-Bio Science Co. Ltd. (China). Tripropylamine (TPrA), mercaptopropionic acid (MPA), tryptophan (Try) and $HAuCl_4{\cdot}3H_2O$ were purchased from Sigma-Aldrich (China). Cucurbit[7]uril, $Zn(CH_3COO)_2{\cdot}2H_2O$, $SnCl_4$, NaOH, progesterone (PRG), kanamycin solution, chloramphenicol (CAP), microcystin (MC), glutaraldehyde (GA) and TE buffer was obtained from Maclin Reagent (China). The milk samples were received from Mengniu Dairy Industry Co., LTD., Tai'an. Honey samples were produced in the Lianhuashan apiary in Xintai City. Ultra-pure water was used throughout the experiment. The aptamer sequence was customized and synthesized by Sangon Biotech (Shanghai) Co., Ltd.. The sequence of aptamers is as follows (from 5 to

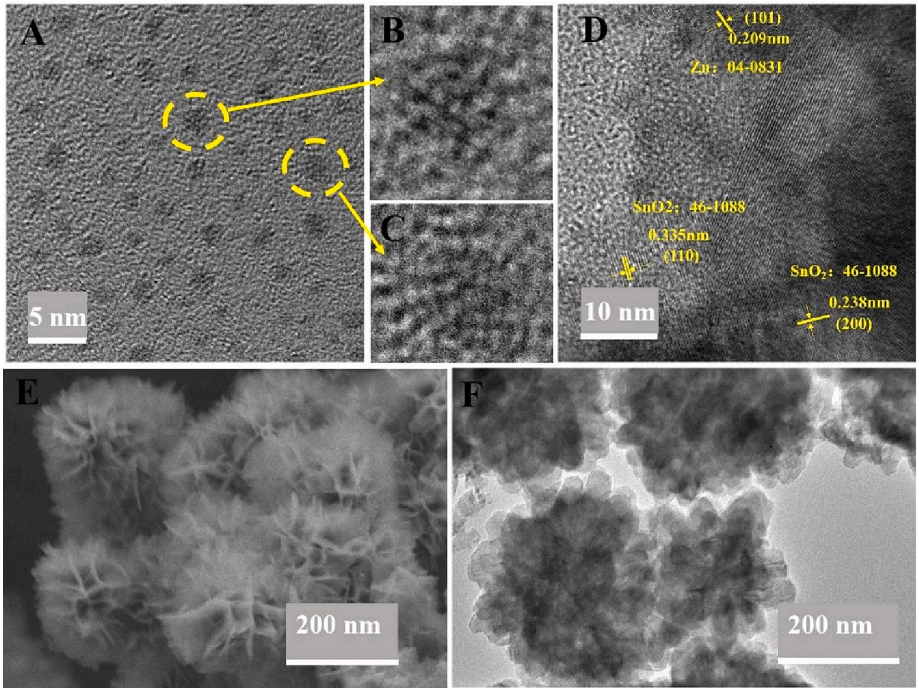

Fig. 1. TEM of cucurbit[7]uril@Try-MPA-gold nanoclusters (A, B, C), HRTEM of Zn-SnO_2 NFs (D), SEM images of Zn-SnO_2 NFs (E), TEM images of Zn-SnO_2 NFs (F).

3):

Aptamer 1 (Apt1): GCTAAGCCGA-NH_2.

Aptamer 2 (Apt2): NH_2-TGGGGGTTGAG.

2.2. Apparatus

The morphology of Zn-SnO_2 NFs was observed by scanning electron microscope (SEM) (Zeiss). The morphology and internal structures of Zn-SnO_2 NFs and cucurbit[7]uril@Try-MPA-gold nanoclusters were characterized by Transmission electron microscope (TEM) (JEOL). The absorption properties of infrared radiation of cucurbit[7]uril@Try-MPA-gold nanoclusters and Try-MPA-gold nanoclusters were measured by FT-IR-410 infrared spectrometer (JASCO). The optical properties of cucurbit[7]uril@Try-MPA-gold nanoclusters were characterized by UV–vis spectrometer (PerkinElmer), LS-45/55 PL spectrometer (PerkinElmer) and a custom-made ECL spectrum analyzer. The diffraction pattern of Zn-SnO_2 NFs was measured by D8 focus diffractometer (Bruker AXS). The information of aptamer conformations was gotten from circular dichroism (CD) spectrum (Applied Photophysics. Ltd). The relevant ECL measurements were performed in the ECL analyzer (Xi'an Remax Analytical Instrument Co., Ltd.). The electrochemical tests were performed using electrochemicaland electrochemical workstation (Zahner Zennium PP211).

2.3. Preparation of Zn-SnO2 NFs

As previously reported (Dou, Sabba, Mathews, Wong, Lam, & Mhaisalkar, 2011), Zn-SnO_2 NFs were synthesized. The specific method was as follows: 0.02 mmol $Zn(CH_3COO)_2{\cdot}2H_2O$, 1 mmol $SnCl_4$, and 15 mmol NaOH were added into a 30 mL mixture of ethanol and ultra-pure water. Mix them well and transfer them to a reactor. After the reaction at 180 °C for 24 h, the obtained product was centrifugally washed several times. Place the product in a vacuum oven to dry. Zn-SnO_2 NFs were amino-functionalized in order to better associate bioactive molecules. 0.1 mL APTES was added to the dispersed product (0.1 g), and then washed and dried after heating in the oil bath.

2.4. Preparation of Cucurbit[7]uril@Try-MPA-Gold nanoclusters

Add 206 μL (2%) of $HAuCl_4$ to 10 mL of ethanol. Mix the solution thoroughly before injecting 0.4 mL of MPA into the mixture. Stir until a colorless dispersion was formed. Add 5 mg Try to the dispersion and continue stirring for 20 min. After adding 5 mg cucurbit[7]uril and stirring for 30 min, cucurbit[7]uril@Try-MPA-gold nanoclusters were formed, and the obtained solution was centrifuged at 10000 rpm. Rinse several times and disperse in 1 mL of ultra-pure water.

2.5. Preparation of Cucurbit[7]uril@Try-MPA-Gold Nanoclusters-Apt2

Apt2 (200 μL, 3.0 μM) was evenly mixed with the prepared cucurbit [7]uril@Try-MPA-gold nanoclusters (100 μL), incubated at room temperature for 6 h, washed and suspended in TE buffer solution (300 μL), stored at 4 °C for later use.

2.6. Fabrication of ECL split aptamer sensors

The working electrodes (glassy carbon electrode (GCE)) were polished and dried in an N_2 atmosphere. Then Zn-SnO2 NFs (8 μL, 1 mg/mL) were dropped. After 60 min, the GA solution (3 μL, 0.5 wt%) was covered on the Zn-SnO_2 NFs surface and incubated for 60 min. Then (6 μL, 5 μM) of Apt1 was cast at room temperature for 60 min and then cleaned with PBS. After that, the inactive sites were blocked with 2 μL 0.1 wt% BSA. After cleaning with PBS, the modified GCE was placed into the solution containing different concentrations of KANA and cucurbit [7]uril@Try-MPA-gold nanoclusters-Apt2 and incubated for 40 min.

2.7. Sample handling procedure

The milk samples were processed in the following way. 5 mL milk was diluted with 90 mL PBS (pH = 7.4), then 5 mL 18 mM $CaCl_2$ was added for mixing, centrifuged at 6000 rpm for 8 min, and the supernatant was collected. Standard concentrations of KANA were added to the treated milk.

The honey sample was treated as follows. The honey sample was diluted tenfold and filtered with a 0.22 μm microporous membrane. A

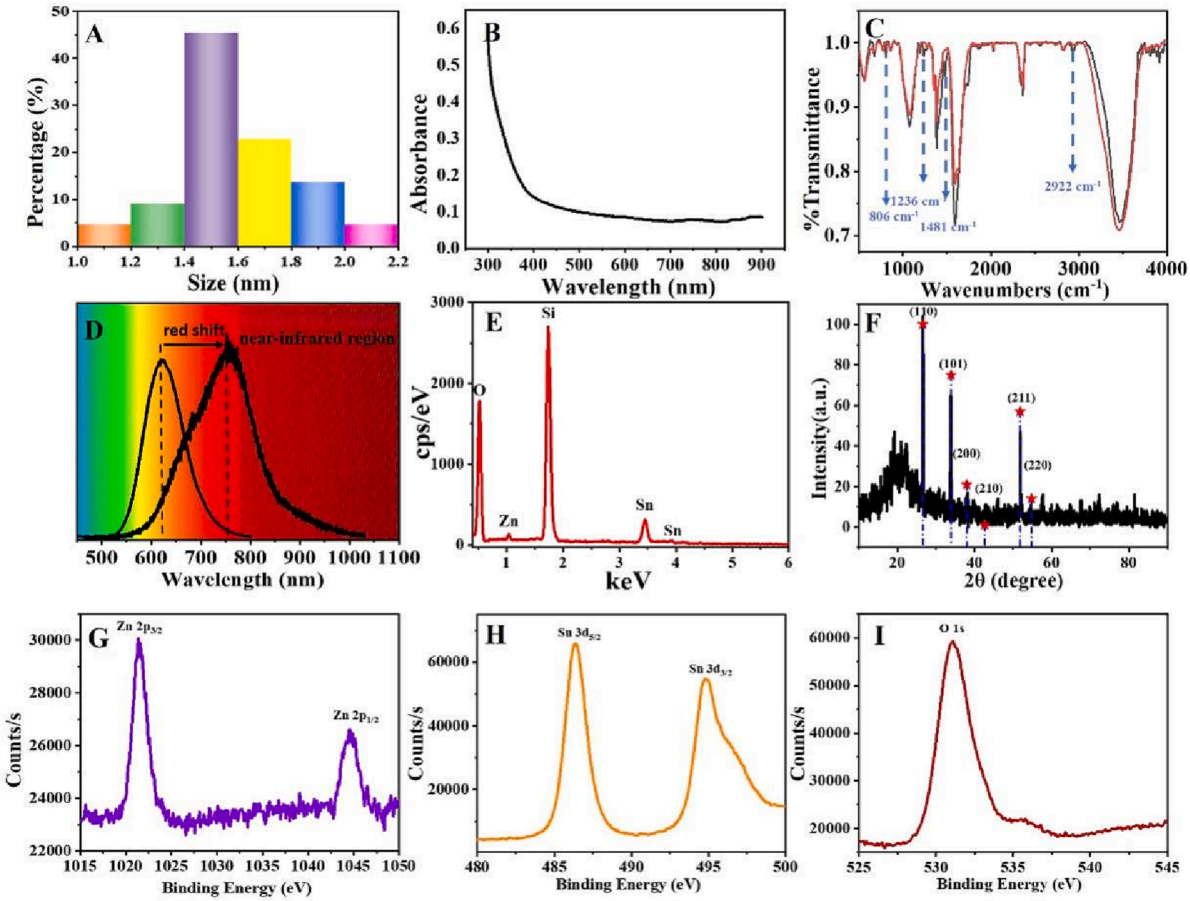

Fig. 2. Size distribution (A) and UV–vis absorption (B) of cucurbit[7]uril@Try-MPA-gold nanoclusters. FT-IR spectra of cucurbit[7]uril@Try-MPA-gold nanoclusters (red curve) and Try-MPA-gold nanoclusters (black curve) (C), PL spectra of cucurbit[7]uril@Try-MPA-gold nanoclusters and ECL spectra of cucurbit[7]uril@Try-MPA-gold nanoclusters in 0.1 M, pH 8.0 PBS containing 15 mM TPrA (D), energy-dispersive X-ray spectroscopy (EDS) (E), XRD pattern (F) and XPS spectra of Zn-SnO_2 NFs: Zn 2p (G), Sn 3d (H), O 1 s (I).

certain concentration of KANA was added to the treated honey samples and mixed evenly.

2.8. Measurement procedure

GCE (**Φ = 4 mm**), platinum wire and Ag/AgCl electrode are used as working electrode, counter electrode, and reference electrode respectively in the ECL test. The electrolyte was 10 mL 0.1 M PBS (pH 8.0) containing 15 mM TPrA. The following parameters were used: the voltage scan range was set from 0 to 1.6 V, and the photomultiplier tube voltage was adjusted to 600 V.

3. Results and discussion

3.1. Characterizations of Cucurbit[7]uril@Try-MPA-Gold nanoclusters

The characterization of the cucurbit[7]uril@Try-MPA-gold nanoclusters was concluded by optical and correlation morphological means. Fig. 1A displayed a TEM image of cucurbit[7]uril@Try-MPA-gold nanoclusters. Part of the cucurbit[7]uril@Try-MPA-gold nanoclusters could show the crystal plane characteristics clearly. The exposed lattice fringes in Figures B and C were from the (2 0 0) and (1 1 1) crystal planes of the Au, respectively. The particle size distributions of cucurbit[7]uril@Try-MPA-gold nanoclusters were displayed in Fig. 2A. The particle sizes of the nanoclusters were generally between 1 and 2.2 nm. Of these, the number of nanoclusters in size range of 1.4 to 1.6 nm was larger, accounting for 45.45 % of the total. The level-spacing gradually increases as the size of the metal particle decreases and that when it decreases to the Fermi wavelength of the electron, the level-spacing splits from the continuum into perpendicular levels. Therefore, the synthesized cucurbit[7]uril@Try-MPA-gold nanoclusters did not have surface plasmon resonance (SPR) absorption peaks (Fig. 2B). Under a certain wavelength of light, the cucurbit[7]uril@Try-MPA-gold nanoclusters could achieve electron transition between energy levels and thus exhibit fluorescence emission from the visible to the near-infrared light region (500 ~ 800 nm) (Fig. 2D). Under the condition of using triethylamine (TPrA) as a co-reactant, the prepared nanoclusters exhibited anode ECL emission that ranged from visible to near-infrared. The maximum ECL emission wavelength was observed at 753 nm, which showed a red-shift compared to the maximum fluorescence emission wavelength. This finding supports the surface state emission model (Jin, Zhu, Wang, Li, Ju, & Lei, 2020) of the cucurbit[7]uril@Try-MPA-gold nanoclusters. The infrared data showed that cucurbit[7]uril had a confinement effect on the surface ligands of the nanoclusters. Specifically, when cucurbit[7]uril was assembled on the surface of the nanoclusters, the out-of-plane bending vibration (806 cm^{-1}) and deformation vibration (1236 cm^{-1}) of the C—H bond of the benzene ring of Try were limited. The absence of the absorption peak at 1481 cm^{-1} and the reduction in the absorption peak at 2922 cm^{-1} indicated that the confinement effect also restrained the tensile deformation of methylene.

3.2. Characterizations of Zn-SnO2 NFs

The morphology of the synthesized Zn-SnO_2 NFs was characterized

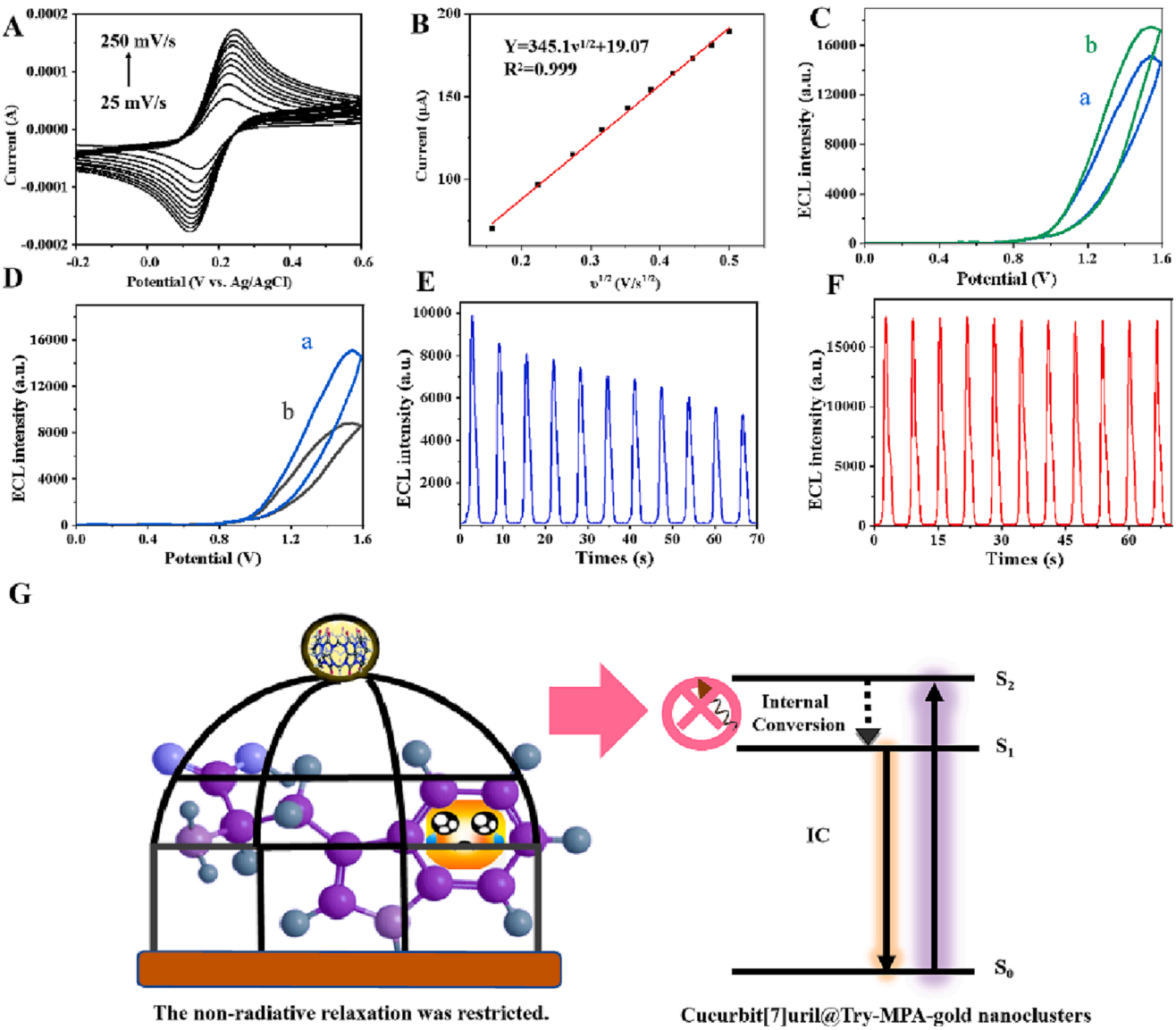

Fig. 3. CV curves (A) and linear relations (B) of GCE modified with Zn-SnO_2 NFs in 5.0 mM $Fe(CN)_6^{3-/4-}$, ECL intensity-potential curves of cucurbit[7]uril@Try-MPA-gold nanoclusters/TPrA (a) and cucurbit[7]uril@Try-MPA-gold nanoclusters/Zn-SnO_2 NFs/TPrA system (b) (C), ECL intensity-potential curves of cucurbit[7]uril@Try-MPA-gold nanoclusters/TPrA (a) and Try-MPA-gold nanoclusters/TPrA system (b) (D), The ECL stability of Try-MPA-gold nanoclusters/Zn-SnO_2 NFs/TPrA system (E) and cucurbit[7]uril@Try-MPA-gold nanoclusters/Zn-SnO_2 NFs/TPrA system (F), schematic illustration for non-covalent bond self-assembly strategy ECL enhancement of cucurbit[7]uril@Try-MPA-gold nanoclusters (G).

by SEM and TEM. Zn-SnO_2 NFs had a uniform flower-like structure with a size ranging from 250 nm to 350 nm (Fig. 1E, F). Lattice fringes of Zn-SnO_2 NFs could be seen under HRTEM, representing the (101) crystal planes of Zn (JCPDS#04-0831) and the (110) and (200) crystal planes of SnO_2 (JCPDS#46-1088), respectively. The elemental analysis also indicated that the nano-flower was composed of the elements Zn, Sn, and O. The X-ray diffraction analysis revealed that the Zn-SnO_2 NFs had excellent crystallinity. The diffraction peaks observed at 26.61°, 33.89°, 37.94°, 42.63°, 51.78°, and 54.76° corresponded to the crystal planes of SnO_2 (110), (101), (200), (210), (211), and (220), respectively. By analyzing the XPS data, additional proof of Zn doping in SnO_2 can be acquired. The binding energies of Zn $2p_{3/2}$ and Zn $2p_{1/2}$ were found to be 1021 eV and 1044 eV, respectively. The binding energy at 486 eV and 494 eV corresponded to Sn $3d_{5/2}$ and Sn $3d_{3/2}$, respectively. The presence of O 1 s orbitals was confirmed by the binding energy at 531 eV.

3.3. Proof of the enhancement of the ECL performance

The electroactive surface area (EASA) has a significant effect to sensitivity of biosensors, thus the EASA of Zn-SnO_2 NFs modified GCE was tested (Fig. 3A, B). The calculation method of EASA is usually based on electrochemical methods. The commonly used method is the Randles-Sevcik equation, whose calculation formula is: $I = 2.69 \times 10^5 A D^{1/2} n^{3/2} v^{1/2} c$, where A represents the EASA, D is the diffusion coefficient of $[Fe(CN)_6]^{4-/3-}$ at room temperature, n is the number of electrons transferred, v is the scan rate, C is the concentration of the $K_3[Fe(CN)_6]$ solution, and I is the peak reduction current of $K_3[Fe(CN)_6]$. Cyclic voltammetry (CV) test was carried out to get the relationship of I and v (Fig. 3A), and the fitting linear was showed as Fig. 3B. The EASA of Zn-SnO_2 NFs modified GCE was calculated as 0.19 cm^2, which is larger than that of the bare GCE (Φ = 4 mm, 0.13 cm^2). Due to the larger EASA, a greater number of electroactive substances can be concentrated on the surface of the electrode, which is significant for sensors with higher sensitivity. When a voltage is applied, more excited molecules are

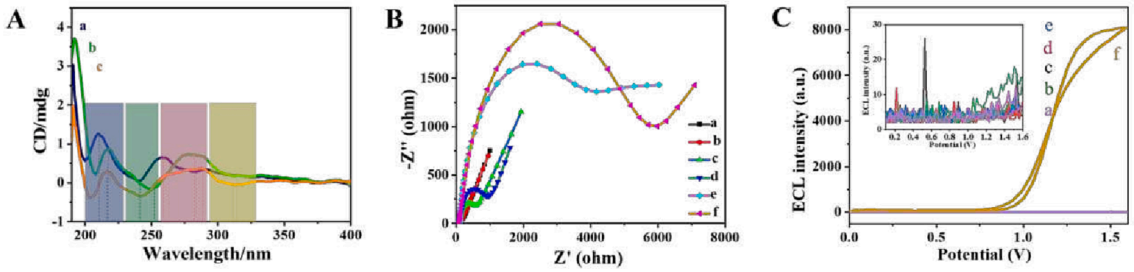

Fig. 4. The CD spectrum of Apt1 (a), cucurbit[7]uril@Try-MPA-gold nanoclusters-Apt 2 (b), and Apt1/KANA/cucurbit[7]uril@Try-MPA-gold nanoclusters-Apt2 (c), (A), EIS curves (B) and ECL intensity-potential curves (C) of GCE (a), Zn-SnO_2 NFs/GCE (b), GA/Zn-SnO_2 NFs/GCE (c), Apt1/GA/Zn-SnO_2 NFs/GCE (d), BSA/Apt1/GA/Zn-SnO_2 NFs/GCE (e), cucurbit[7]uril@Try-MPA-gold nanoclusters-Apt2/KANA/BSA/Apt1/GA/Zn-SnO_2 NFs/GCE (f).

generated, resulting in an enhanced ECL emission. As shown in Fig. 3C, the ECL intensity of the system with Zn-SnO_2 NFs as the substrate material was enhanced by approximately 2328 a.u.

The effect of the non-covalent bond self-assembly strategy on enhancing ECL performance was investigated (Fig. 3D). The ECL intensity of gold nanoclusters synthesized with Try and MPA as ligands was found to be approximately 8800 a.u. (curve b). Surprisingly, under the effect of the non-covalent bond self-assembly strategy, the luminous intensity of the nanoclusters increased to 15,161 a.u. (curve a), which was 72% higher than that before cucurbit[7]uril treatment. Non-radiative relaxation affects the luminescence of the material. The infrared data suggest that the cavity of cucurbit[7]uril acts as a molecular cage, which enhances the nanoclusters' ECL emission intensity by inhibiting Try's non-radiative relaxation (Fig. 3G). Furthermore, many dangling bonds may form non-radiative transition channels on the surface of Try-MPA-gold nanoclusters, which can affect the interaction of active intermediates and the radiation relaxation of excited states. Cucurbit[7]uril can form supramolecular structure with Try-MPA-gold nanoclusters to reduce the influence of surface effect on ECL luminescence.

The ECL stability of Try-MPA-gold nanoclusters/Zn-SnO_2 NFs/TPrA system (Fig. 3E) and cucurbit[7]uril@Try-MPA-gold nanoclusters/Zn-SnO_2 NFs/TPrA system (Fig. 3F) was investigated. Nanoclusters treated with a non-covalent bond self-assembly strategy exhibited better stability. The improved ECL stability could be attributed to the enhanced stability and dispersion of the nanoclusters in the aqueous phase.

3.4. Possible ECL mechanism

The cucurbit[7]uril@Try-MPA-gold nanoclusters undergo oxidation reactions and form cucurbit[7]uril@Try-MPA-gold nanoclusters$^{\bullet+}$. TPrA was electrochemically oxidized to produce a short-lived free radical (TPrA$^{\bullet+}$) and then formed a strong reducing intermediate (TPrA$^{\bullet}$) by losing a proton on α-C. TPrA$^{\bullet}$ provided an electron to generate cucurbit[7]uril@Try-MPA-gold nanoclusters*, which subsequently relaxed to the ground state and emitted ECL emission.

cucurbit[7]uril@Try-MPA-gold nanoclusters $-e^{-}\rightarrow$ cucurbit[7]uril@Try-MPA-gold nanoclusters $^{\bullet+}$ (1)

TPrA $- e^{-} \rightarrow$ TPrA $^{\bullet+}$ (2)

TPrA$^{\bullet+}$+$OH^{-}\rightarrow$ TPrA$^{\bullet}$+H_2O (3)

cucurbit[7]uril@Try-MPA-gold nanoclusters $^{\bullet+}$ + TPrA$^{\bullet}\rightarrow$cucurbit[7]uril@-Try-MPA-gold nanoclusters*+TPrA (4)

cucurbit[7]uril@Try-MPA-gold nanoclusters*$\rightarrow$ cucurbit[7]uril@Try-MPA-gold nanoclusters + hν (5)

3.5. Feasibility of split aptamer sensors

To validate the feasibility of the KANA split aptamer sensor, the following experiments were conducted. CD is a useful tool for investigating conformational changes in DNA (Figueroa-DePaz, Resendiz-Acevedo, Dávila-Manzanilla, García-Ramos, Ortiz-Frade, Serment-Guerrero, et al., 2022; Liu, Xia, Yu, Gu, Yuan, Liu, et al., 2022). Changes in DNA conformation lead to changes in the coupling of the electronic transition dipole moments of the DNA bases and shift the wavelength position of the original CD peak (Yamashita, Miyazaki, Yamaguchi, Briones, Nakamura, & Maeda, 2008). Neither Apt1 nor cucurbit[7]uril@Try-MPA-gold nanoclusters-Apt2 could independently identify kanamycin. When KANA was introduced separately to Apt1 or cucurbit[7]uril@Try-MPA-gold nanoclusters-Apt2, it did not induce any conformational changes (Fig. S2). As depicted in Fig. 4A, the CD spectrum of Apt1 (curve a) exhibited negative peaks at 200 nm and 240 nm and positive peaks at 209 nm and 258 nm. Cucurbit[7]uril@Try-MPA-gold nanoclusters -Apt2 had negative peaks at 208 nm and 250 nm, and positive peaks at 217 nm and 276 nm. Upon interaction with KANA, the positive and negative peaks of the CD spectra shifted, indicating that the binding interaction between KANA and aptamers induced conformational changes in the aptamers. This suggests that Apt1 and cucurbit[7]uril@Try-MPA-gold nanoclusters-Apt2 can jointly identify KANA.

Electrochemical impedance spectroscopy (EIS) is an effective method for characterizing the properties of modified electrode surfaces (Ciucci, 2019) and studying sensor construction procedures (Mi, Li, Tan, & Tu, 2020; Xin, Jiang, Zong, Zeng, Shu, Marks, et al., 2018). As shown in Fig. 4B, the radius of the semicircle part in the EIS of the bare GCE was small (curve a). After modification with Zn-SnO_2 NFs, the radius of the semicircle part in the EIS corresponding to the charge transfer resistance did not exhibit significant changes (curve b). GA modification to the electrode surface obstructed charge transfer between the anionic probe $[Fe(CN)_6]^{3-/4-}$ and the electrode surface (curve c). Modification of Apt1 on the electrode surface resulted in a significant increase in the radius of the semicircle part in the EIS (curve d). This effect may be attributed to the phosphoric acid backbone of Apt1, which can hinder charge transfer between the anionic probe $[Fe(CN)_6]^{3-/4-}$ and the electrode surface, leading to an increase in charge transfer resistance. BSA blocking the non-specific active site further increased charge transfer resistance due to protein blocking electron transport (curve e). Impedance further increased when KANA was captured on the electrode surface by cucurbit[7]uril@Try-MPA-gold nanoclusters-Apt2 and Apt1 (curve f).

We used the ECL method to verify the process of sensor assembly (Fig. 4D). The assembly of Zn-SnO_2 NFs, GA, Apt1, and BSA on the electrode did not affect ECL emission. Successful capture of KANA by Apt1 and cucurbit[7]uril@Try-MPA-gold nanoclusters-Apt2 on the electrode surface was evidenced by the detection of ECL signal from the nanoclusters, providing strong evidence for successful construction of the ECL split aptamer sensor.

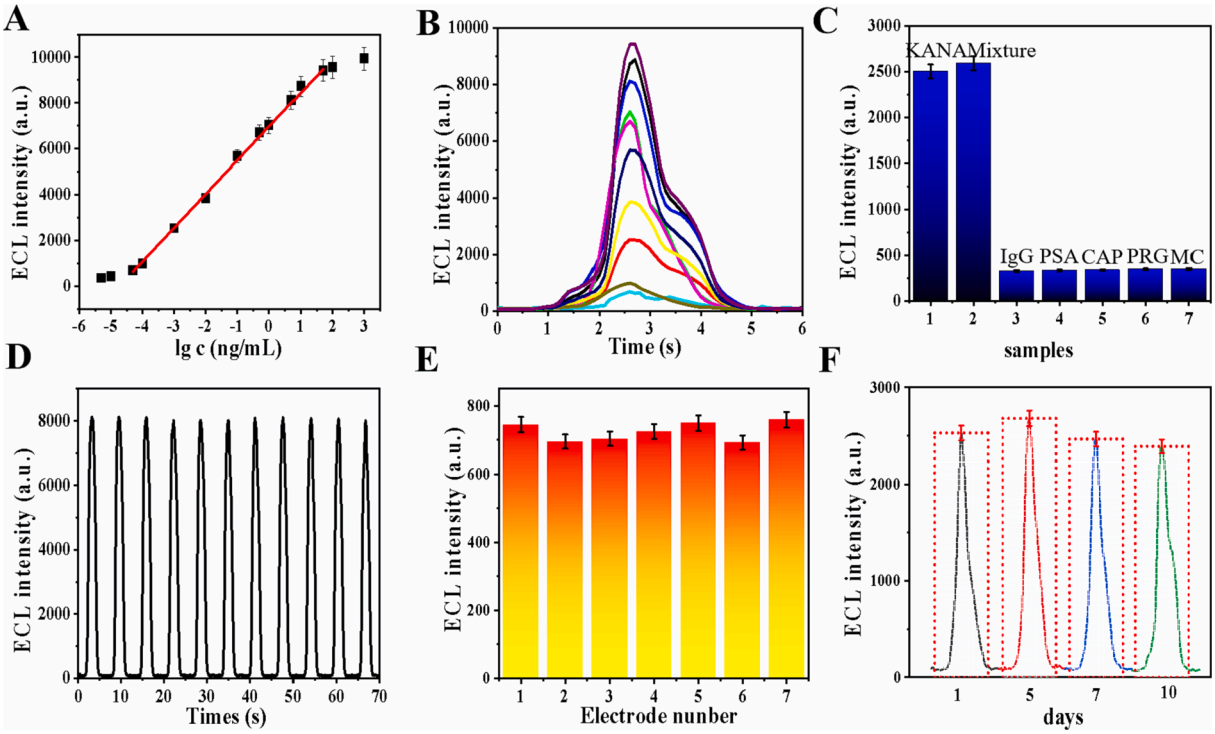

Fig. 5. Calibration (A) and ECL intensity (B) of the split aptamer sensors at different concentrations of KANA. Selectivity (C) and operational stability under consecutive scanning (D), reproducibility (E), and positioned stability of the split aptamer sensors (F). Error bars: ±standard deviation (SD), $n = 5$.

Table 1
Recoveries of KANA in samples based on the proposed ECL sensor.

Samples	Addition (ng/mL)	Average (ng/mL, $n = 11$)	RSD (%)	Recovery (%)
Milk	0.0100	0.0102	4.7	102.0
	0.100	0.101	4.9	101.0
	1.00	1.06	4.4	106.0
Honey	0.0100	0.0101	4.9	101.0
	0.100	0.104	2.7	104.0
	1.00	0.962	2.8	96.2

3.6. Evaluation of the methodology for KANA detection

Under optimal conditions (Fig. S1), the split aptamer sensor was used to measure KANA standard solutions. It was found that the logarithmic value (*lgC*) of KANA concentration was linearly correlated with the ECL response value (*I*) in the range of 50.00 fg/mL to 50.00 ng/mL. The linear regression equation was $I = 1473\ lgC + 6970$, $R^2 = 0.998$, and the lowest detection limit (LOD) was 32.90 fg/mL. The specificity of the KANA split aptamer was tested using IgG, PSA, CAP, PRG, and MC as interferences. As shown in Fig. 5C, when these substances were used as interferences, the sensor did not generate a signal response. When a mixture of CAP and KANA was tested, the sensor specifically recognized KANA and produced a corresponding ECL signal. The sensor was scanned continuously for 11 cycles between 0 and 1.6 V to measure the signal response to 5 ng/mL KANA. The results showed that the obtained RSD was 0.5%, demonstrating good operational stability (Fig. 5D). The ECL signal test was carried out on seven modified electrodes simultaneously, and it was found that the signal intensity expressed by the seven electrodes did not vary significantly (RSD = 3.8%), indicating good reproducibility of the sensor (Fig. 5E). To test the storage stability of the ECL sensor, it was placed in the refrigerator for 10 days, and its ECL signal strength changed little (Fig. 5F).

3.7. Analysis of the samples

To investigate the practicability of the method, we tested the KANA concentration by adding a certain concentration of KANA to milk and honey samples using a standard addition method. The milk and honey samples were tested by LC-MS/MS, which showed no KANA residue in the samples. As shown in Table 1, the recovery rate of KANA in milk ranges from 101.0% to 106.0%, with RSD between 4.4% and 4.9%. The recovery rate of KANA in honey ranges from 96.2% to 104.0%, with RSD between 2.7% and 4.9%. The constructed split aptamer sensor can be applied in complex food substrates based on these results.

4. Conclusion

In this study, we utilized a non-covalent bond self-assembly strategy to improve the ECL performance of the anode signal probe. The tailored aptamer was used as the capture probe, which offers the possibility to stabilize the aptamer structure and improve the accessibility of the aptamer sensor design. Combined with the large specific surface area and high electron mobility of Zn-SnO_2 NFs, a split aptamer sensor for detecting KANA was successfully constructed. The split aptamer sensor developed in this study can detect KANA with high sensitivity and accuracy in complex food substrates.

CRediT authorship contribution statement

Xiaoyue Zhang: Conceptualization, Data curation, Writing – original draft. **Yu Du:** Methodology, Data curation. **Xuejing Liu:** Data curation, Writing – review & editing. **Rui Feng:** Writing – review & editing. **Yue Jia:** Methodology, Writing – review & editing. **Xiang Ren:** Methodology. **Nuo Zhang:** Formal analysis. **Lei Liu:** Formal analysis. **Qin Wei:** Funding acquisition, Formal analysis. **Huangxian Ju:** Funding acquisition, Formal analysis.

Declaration of Competing Interest

The authors declare that they have no known competing financial interests or personal relationships that could have appeared to influence the work reported in this paper.

Data availability

No data was used for the research described in the article.

Acknowledgements

This study was supported by the National Natural Science Foundation of China (No.22274062, 22206056), the Shandong Provincial Natural Science Foundation (No. ZR2020QB097), Jinan Scientific Research Leader Workshop Project (2019GXRC027), Special Foundation for Taishan Scholar Professorship of Shandong Province.

Appendix A. Supplementary data

Supplementary data to this article can be found online at https://doi.org/10.1016/j.foodchem.2023.136083.

References

Cheng, S., Zhang, H., Huang, J., Xu, R., Sun, X., & Guo, Y. (2020). Highly sensitive electrochemiluminescence aptasensor based on dual-signal amplification strategy for kanamycin detection. *Science of The Total Environment, 737*, 139785.

Ciucci, F. (2019). Modeling electrochemical impedance spectroscopy. *Current Opinion in Electrochemistry, 13*, 132–139.

Debiais, M., Lelievre, A., Smietana, M., & Müller, S. (2020). Splitting aptamers and nucleic acid enzymes for the development of advanced biosensors. *Nucleic Acids Research, 48*(7), 3400–3422.

Dou, X., Sabba, D., Mathews, N., Wong, L. H., Lam, Y. M., & Mhaisalkar, S. (2011). Hydrothermal synthesis of high electron mobility Zn-doped SnO_2 nanoflowers as photoanode material for efficient dye-sensitized solar cells. *Chemistry of Materials, 23*(17), 3938–3945.

El-Barghouthi, M. I., Bodoor, K., Abuhasan, O. M., Assaf, K. I., Al Hourani, B. J., & Rawashdeh, A. M. M. (2022). Binary and ternary complexes of cucurbit[8]uril with tryptophan, phenylalanine, and tyrosine: A computational study. *ACS Omega, 7*(12), 10729–10737.

Figueroa-DePaz, Y., Resendiz-Acevedo, K., Dávila-Manzanilla, S. G., García-Ramos, J. C., Ortiz-Frade, L., Serment-Guerrero, J., & Ruiz-Azuara, L. (2022). DNA, a target of mixed chelate copper(II) compounds (Casiopeinas®) studied by electrophoresis, UV–vis and circular dichroism techniques. *Journal of Inorganic Biochemistry, 231*, 111772.

Guan, Z.-J., Li, J.-J., Hu, F., & Wang, Q.-M. (2022). Structural engineering toward gold nanocluster catalysis. *Angewandte Chemie International Edition, 61*, e202209725.

He, G., Huang, P., & Chen, X. (2020). Theranostic multimodal gold nanoclusters. *Nature Biomedical Engineering, 4*(7), 668–669.

Hu, J., Song, H., Zhou, J., Liu, R., & Lv, Y. (2021). Metal-tagged CRISPR/Cas12a bioassay enables ultrasensitive and highly selective evaluation of kanamycin bioaccumulation in fish samples. *Analytical Chemistry, 93*(42), 14214–14222.

Huang, Z., Li, Z., Chen, Y., Xu, L., Xie, Q., Deng, H., … Peng, H. (2021). Regulating valence states of gold nanocluster as a new strategy for the ultrasensitive electrochemiluminescence detection of kanamycin. *Analytical Chemistry, 93*(10), 4635–4640.

Jiang, D., Qin, M., Zhang, L., Shan, X., & Chen, Z. (2021). Ultrasensitive all-solid-state electrochemiluminescence platform for kanamycin detection based on the pore confinement effect of 0D g-C3N4 quantum dots/3D graphene hydrogel. *Sensors and Actuators B: Chemical, 345*, 130343.

Jin, Z., Zhu, X., Wang, N., Li, Y., Ju, H., & Lei, J. (2020). Electroactive metal-organic frameworks as emitters for self-enhanced electrochemiluminescence in aqueous medium. *Angewandte Chemie International Edition, 59*(26), 10446–10450.

Li, P., Luo, L., Cheng, D., Sun, Y., Zhang, Y., Liu, M., & Yao, S. (2022). Regulation of the structure of zirconium-based porphyrinic metal-organic framework as highly electrochemiluminescence sensing platform for thrombin. *Analytical Chemistry, 94*(14), 5707–5714.

Liu, Q., Xia, J., Yu, Q., Gu, P., Yuan, Y., Liu, K., … Qian, H. (2022). Engineering the surface properties of DNA nanostructures by tuning the valency of assembling species for biomedical applications. *Macromolecular Bioscience, 22*(11), 2200248.

Matus, M. F., & Häkkinen, H. (2021). Gold nanoclusters: Atomically precise gold nanoclusters: Towards an optimal biocompatible system from a theoretical-experimental strategy. *Small, 17*(27), 2170140.

Mi, X., Li, H., Tan, R., & Tu, Y. (2020). Dual-modular aptasensor for detection of cardiac troponin I based on mesoporous silica films by electrochemiluminescence/Electrochemical impedance spectroscopy. *Analytical Chemistry, 92*(21), 14640–14647.

Qi, S., Dong, X., Sun, Y., Zhang, Y., Duan, N., & Wang, Z. (2022). Split aptamer remodeling-initiated target-self-service 3D-DNA walker for ultrasensitive detection of 17β-estradiol. *Journal of Hazardous Materials, 439*, 129590.

Robati, R. Y., Arab, A., Ramezani, M., Langroodi, F. A., Abnous, K., & Taghdisi, S. M. (2016). Aptasensors for quantitative detection of kanamycin. *Biosensors and Bioelectronics, 82*, 162–172.

Tian, D., Wang, J., Zhuang, Q., Wu, S., Yu, Y., & Ding, K. (2023). An electrochemiluminescence biosensor based on Graphitic carbon nitride luminescence quenching for detection of AFB1. *Food Chemistry, 404*, 134183.

Wang, H., Wang, Y., Cai, L., Liu, C., Zhang, B., Fang, G., & Wang, S. (2022). Polythionine-mediated AgNWs-AuNPs aggregation conductive network: Fabrication of molecularly imprinted electrochemiluminescence sensors for selective capture of kanamycin. *Journal of Hazardous Materials, 434*, 128882.

Wang, R., Zhang, Q., Zhang, Y., Shi, H., Nguyen, K. T., & Zhou, X. (2019). Unconventional split aptamers cleaved at functionally essential sites preserve biorecognition capability. *Analytical Chemistry, 91*(24), 15811–15817.

Wang, Y., Feng, D., & Kan, X. (2022). The combination of highly efficient resonance energy transfer in one nanocomposite and ferrocene-quenching for ultrasensitive electrochemiluminescence bioanalysis. *Biosensors and Bioelectronics, 210*, 114347.

Xin, W.-L., Jiang, L.-F., Zong, L.-P., Zeng, H.-B., Shu, G.-F., Marks, R., … Shan, D. (2018). MoS_2 quantum dots-combined zirconium-metalloporphyrin frameworks: Synergistic effect on electron transfer and application for bioassay. *Sensors and Actuators B: Chemical, 273*, 566–573.

Yamashita, K., Miyazaki, M., Yamaguchi, Y., Briones, M. P., Nakamura, H., & Maeda, H. (2008). Direct circular dichroism spectra measurement of stretching long-strand DNA in a tapering microchannel. *Chemical Engineering Journal, 135*, S288–S291.

Ye, H., Yang, Z., Khan, I. M., Niazi, S., Guo, Y., Wang, Z., & Yang, H. (2022). Split aptamer acquisition mechanisms and current application in antibiotics detection: A short review. *Critical Reviews in Food Science and Nutrition*, 1–12.

Yu, L., Zhang, Q., Kang, Q., Zhang, B., Shen, D., & Zou, G. (2020). Near-infrared electrochemiluminescence immunoassay with biocompatible au nanoclusters as tags. *Analytical Chemistry, 92*(11), 7581–7587.

Zhang, N., Wang, X.-T., Xiong, Z., Huang, L.-Y., Jin, Y., Wang, A.-J., … Feng, J.-J. (2021). Hydrogen bond organic frameworks as a novel electrochemiluminescence luminophore: Simple synthesis and ultrasensitive biosensing. *Analytical Chemistry, 93*(51), 17110–17118.

Zhao, L., Qi, X., Yan, X., Huang, Y., Liang, X., Zhang, L., … Tan, W. (2019). Engineering aptamer with enhanced affinity by triple helix-based terminal fixation. *Journal of the American Chemical Society, 141*(44), 17493–17497.

Zheng, Y., Wu, J., Jiang, H., & Wang, X. (2021). Gold nanoclusters for theranostic applications. *Coordination Chemistry Reviews, 431*, 213689.